Supporting Information

A Tetrahedrally Coordinated $L_3Fe\text{-}N_x$ Platform that Accommodates Terminal Nitride ($Fe^{IV}\equiv N$) and Dinitrogen ($Fe^{I}\text{-}N_2\text{-}Fe^{I}$) Ligands

Theodore A. Betley and Jonas C. Peters*

Division of Chemistry and Chemical Engineering Arnold and Mabel Beckman Laboratories of Chemical Synthesis,

California Institute of Technology

Pasadena, California 91125

Experimental Section

All manipulations were carried out using standard Schlenk or glove-box techniques under a dinitrogen atmosphere or argon atmosphere when indicated. Unless otherwise noted, solvents were deoxygenated and dried by thorough sparging with N_2 gas followed by passage through an activated alumina column. Non-halogenated solvents were typically tested with a standard purple solution of sodium benzophenone ketyl in tetrahydrofuran in order to confirm effective oxygen and moisture removal. Deuterated solvents were degassed and stored over activated 3-Å molecular sieves prior to use. THF-d_8 was dried by passage over activated alumina and stored over activated sieves prior to use. [$PhBP^{iPr}_3$]FeCl,[1] Hdbabh (dbabh = 2,3:5,6-dibenzo-7-aza bicyclo[2.2.1]hepta-2,5-diene),[2] and Li(dbabh)[3] were prepared as previously reported. All reagents were purchased from commercial vendors and used without further purification unless explicitly stated. Elemental analyses were carried out at Desert Analytics, Tucson, Arizona. NMR spectra were recorded at ambient temperature on Varian Mercury 300 MHz, Joel 400 MHz, and an Inova 500 MHz spectrometers, unless otherwise noted. ^{1}H NMR chemical shifts were referenced to residual solvent. ^{31}P NMR and ^{15}N NMR chemical shifts are reported relative to an external standard of 85% H_3PO_4 (0 ppm) and CH_3NO_2 (380 ppm relative to liquid ammonia at 0 ppm). GC-MS data was obtained by injecting a dichloromethane solution into an Agilent 6890 GC equipped with an Agilent 5973 mass selective detector (EI). IR spectra were recorded on a Bio-Rad Excalibur FTS 3000 spectrometer controlled by Win-IR Pro software. UV-vis measurements were taken on a Hewlett Packard 8452A diode array spectrometer using a quartz crystal cell with a Teflon cap. X-ray diffraction studies were carried out in the Beckman Institute (Caltech) Crystallographic Facility on a Bruker Smart 1000 CCD diffractometer.

X-ray Crystallography. X-ray quality crystals were grown as indicated in the experimental procedures for each complex. The crystals were mounted on a glass fiber with Paratone-N oil. Structures were determined using direct methods with standard Fourier techniques using the Bruker AXS software package. In some cases, Patterson maps were used in place of the direct methods procedure to generate initial solutions.

^{15}N-Hdbabh: ^{15}N-potassium phthalimide (98%, Aldrich) (5g, 26.8 mmol) was added to a solution of benzylbromide (4.86 g, 28.4 mmol) in DMF (35 mL) in a 250 mL round-bottom flask in air. The solution was heated to 125 ºC for 12 h. Upon cooling the solution to room temperature, 200 mL of cold water was added to the reaction vessel which precipitated the benzylated phthalimide as a white solid. The solids were collected by filtration over a fritted glass funnel and washed with 1.5 L of water. The solids were dried in vacuum over 18 h to yield 6.27 g (98%) of the benzylated phthalimide (GC-MS, ^{1}H NMR). The ^{15}N-Hdbabh was then prepared following the method of Carpino et al.[2] and lithiated according to Mindiola et al.[3] ^{1}H NMR (C_6D_6, 300 MHz): δ 7.04 (m, 4H), 6.76 (m, 4H), 4.88 (d, $^2J_{N\text{-}H}$ = 2.7 Hz, 2H), 2.65 (bs, 1H, N-H). ^{15}N {^{1}H} NMR (C_6D_6, 50.6 MHz): δ 115 ppm. GC-MS (m/z): 194 (M).

[$PhBP^{iPr}_3$]Fe≡N: A thawing solution of [$PhBP^{iPr}_3$]FeCl (60 mg, 0.105 mmol) in THF (0.2 mL) was added to solid Li(dbabh) (20.9 mg, 0.105 mmol) at ca. -100 ºC (*note*: a similar procedure

[1] T. A. Betley, J. C. Peters, *Inorg. Chem.* **42**, 5074 (2003).
[2] L. A. Carpino, R. E. Padykula, D. E. Barr, F. H. Hall, J. G. Krause, R. F. Dufresne, C. J. Thoman, *J. Org. Chem.* **53**, 2565 (1988).
[3] D. J. Mindiola, C. C. Cummins, *Angew. Chem. Int. Ed.* **37**, 945 (1998).

was performed using ^{15}N-Li(dbabh) to generate [PhBP$^{iPr}_3$]Fe≡^{15}N). The solution was stirred vigorously and allowed to warm to room temperature and stirred for an additional 15 minutes. The solution color changed from yellow [PhBP$^{iPr}_3$]FeCl to red as the amide [PhBP$^{iPr}_3$]Fe(dbabh) formed at low temperature (UV-vis for [PhBP$^{iPr}_3$]Fe(dbabh) in THF: λ_{max} = 467 nm (2300 M^{-1} cm^{-1})). After 15 minutes the solution was chilled to -35 ºC and placed under vacuum for 6 h, after which time the resulting red oil was triturated three times with pentane, then evaporated to dryness (2 h under vacuum) while maintaining the temperature at -35 ºC the entire time. To obtain satisfactory IR spectra in pentane the solids were then dissolved in pentane (3 mL), and the resulting solution was allowed to warm to room temperature to generate [PhBP$^{iPr}_3$]Fe≡N and anthracene. The pentane solution was filtered through a glass-fiber filter to remove insoluble material (LiCl) and IR spectra for both [PhBP$^{iPr}_3$]Fe≡N and [PhBP$^{iPr}_3$]Fe≡^{15}N were obtained from ca. equimolar solutions: (Pentane/KBr) ν(Fe≡N) = 1034 cm^{-1}; ν(Fe≡^{15}N) = 1007 cm^{-1}.

^{1}H and ^{31}P NMR data: Alternatively, the red solid residue containing [PhBP$^{iPr}_3$]Fe(dbabh) and LiCl was dissolved in C_6D_6 (0.7 mL), warmed to room temperature, and filtered through a glass-fiber filter to remove salts. After a period of ca. ^{1}H and ^{31}P NMR spectra of the sample were recorded at room temperature (see Figure A1 below): ^{1}H NMR (C_6D_6, 300 MHz): δ 8.13 (s, 2H, $C_{14}H_{14}$), 7.79 (m, 4H, $C_{14}H_{14}$), 7.60 (m, 2H, H_{ortho} BPh), 7.38 (t, 2H, H_{meta} BPh), 7.25 (m, 4H, $C_{14}H_{14}$), (H_{para} BPh obscured by anthracene), 2.10 (septet, 6H, P(C*H*$(CH_3)_2$), 1.45 (dd, J = 7.5, 15.6 Hz, 18H, P(CH(C*H*$_3$)$_2$), 1.24 (dd, J = 7.5, 12.3 Hz, 18H, P(CH(C*H*$_3$)$_2$), 1.00 (m, 6H, B(C*H*$_2$PR$_2$)). ^{31}P {^{1}H} NMR (C_6D_6, 121.4 MHz): δ 84.

^{15}N NMR data: [PhBP$^{iPr}_3$]FeCl (30 mg, 0.052 mmol) and solid ^{15}N-Li(dbabh) (10.5 mg, 0.052 mmol) were added to an NMR tube fitted with a Teflon screw-cap with a capillary tube containing O=P(OMe)$_3$ (7.3 mg, 0.052 mmol) in *d*$_8$-toluene as an internal standard. Thawing THF (0.7 mL) was added to the combined solids in the NMR tube at ca. -100 ºC. The slurry was warmed to -42 ºC in a dry ice/acetonitrile bath. The NMR tube was then inserted into an NMR probe that had been precooled to -45 ºC. The instrument was warmed to -15 ºC to facilitate the amide metathesis reaction. After 30 minutes, the [PhBP$^{iPr}_3$]FeCl had been consumed as ascertained by a ^{1}H NMR spectrum and the instrument was then warmed to 22 ºC ca. 30 minutes to allow [PhBP$^{iPr}_3$]Fe(^{15}N-dbabh) to decay to a significant quantity of [PhBP$^{iPr}_3$]Fe≡^{15}N. The production of [PhBP$^{iPr}_3$]Fe≡^{15}N was monitored via ^{31}P NMR and deemed 85% complete ca. 30 minutes (integrating vs. internal standard). At this time the instrument was cooled to -5 ºC (to minimize bimolecular nitride degradation) and the ^{15}N NMR spectrum was acquired over a period of 8 h. ^{15}N {^{1}H} NMR (THF, 50.751 MHz): δ 952 ppm.

Figure A1. ^{1}H NMR of [PhBP$^{iPr}_3$]Fe≡N in C_6D_6 (scale in ppm) with proton positions labeled.

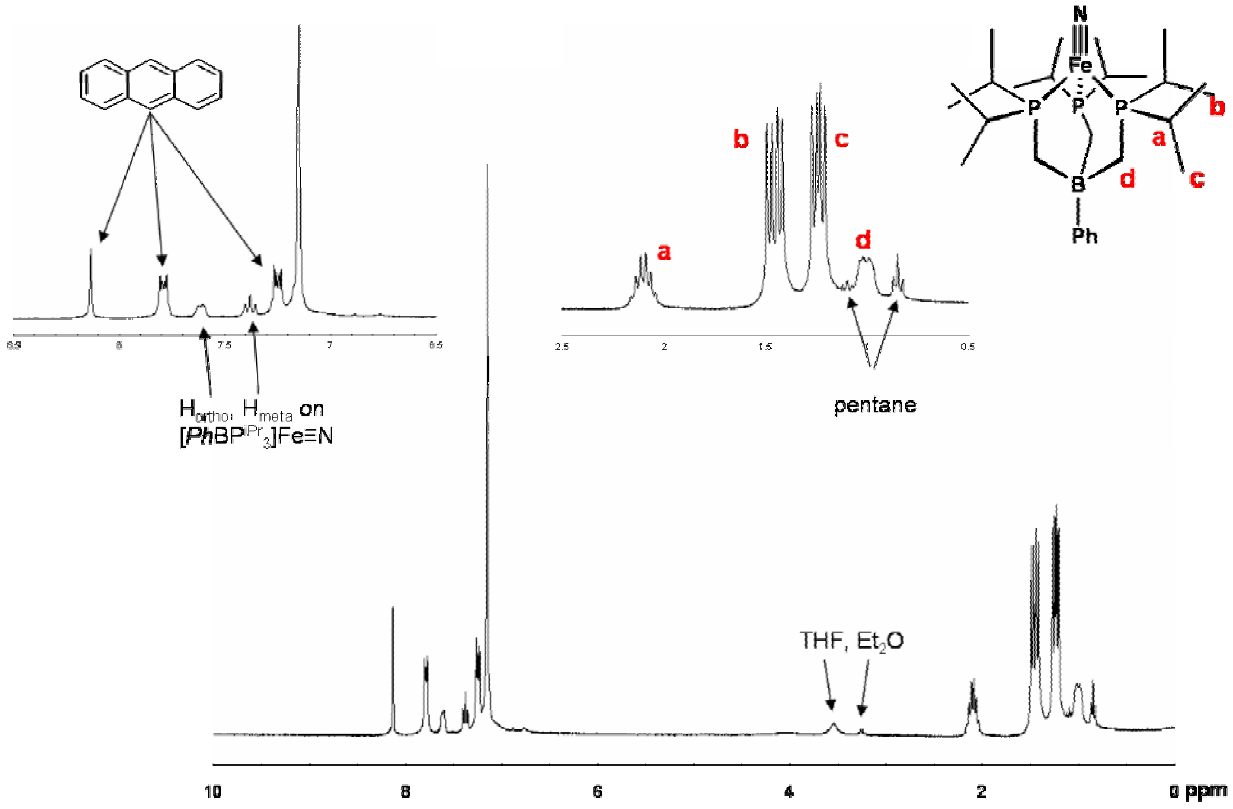

[PhBP$^{iPr}_3$]Fe(NPh$_2$): A thawing solution of [PhBP$^{iPr}_3$]FeCl (40 mg, 0.070 mmol) in THF (0.2 mL) was added to solid Ph$_2$NLi (12.3 mg, 0.072 mmol) at ca. -100 ºC. The solution was then stirred vigorously and allowed to warm to room temperature for 45 minutes. The solution color changed from yellow [PhBP$^{iPr}_3$]FeCl to wine-red as the amide was formed (UV-vis for [PhBP$^{iPr}_3$]Fe(NPh$_2$) (THF) λ_{max} = 450 (1700 M^{-1} cm^{-1})). The volatiles were then removed under vacuum to leave behind a red solid which was then dissolved in pentane (5 mL) and filtered through glass-fiber filter paper to remove salts. Crystals were grown by storing this pentane solution at -35 ºC for 3 days. A single crystal was selected from the batch and used for an X-ray diffraction study (see Figure 7). The mother liquor was decanted from the batch of crystals which were dried in vacuo to yield the product (35.5mg, 72%). ^{1}H NMR (C$_6$D$_6$, 300 MHz): δ 52.99, 42.57, 20.33, 18.75, 6.78, -0.91, -20.57, -33.30, -55.80. Analyzed for C$_{39}$H$_{63}$BFeNP$_3$ calculated (found): C, 66.39 (66.31); H, 9.00 (8.89); N, 1.99 (1.76).

(Trans-[1,2-cyclohexanediamino-N,N'-bis(4-diethylaminosalicylidene])Mn^V≡N: A modified salen ligand trans-[1,2-cyclohexanediamino-N,N'-bis(4-diethylaminosalicylidene] (abbrev. as salen*) was synthesized by refluxing 4-(diethylamino)salicylaldehyde (2 g, 10.2 mmol) and trans-1,2-diaminocyclohexane (590 mg, 5.2 mmol) in ethanol (150 mL) for 2 h. Cooling the solution to room temperature precipitated the salen* as yellow crystals. The yellow crystals were collected on a sintered glass frit and dried under vacuum (2 g, 84%). ^{1}H NMR (C$_6$D$_6$, 300 MHz): δ 7.96 (s, 2H), 6.84 (d 2H), 6.37 (d, 2H), 5.91 (dd, 2H), 2.9 (m, 2H), 2.8 (q, 8H), 1.7 (d, 2H), 1.53 (m, 4H), 1.15 (m, 2H), 0.75 (t, 12H). Following the protocol established by Du Bois et al.,[4] the complex (salen*)Mn≡N was prepared using salen* (2 g, 4.3 mmol), Mn(OAc)$_2$ (1.108 g, 4.5 mmol), NH$_4$OH (4.3 mL, 15 M), and NaOCl (55.5 mL, 0.7 M). The complex (salen*)Mn≡N was additionally purified by filtration through a silica plug in 250 mL of CH$_2$Cl$_2$, followed by removal of the solvent and thorough drying under vacuum (1.96 g, 85.7%). ^{1}H NMR (CD$_2$Cl$_2$, 300 MHz): δ 7.73 (d, 2H), 7.02 (dd, 2H), 6.14 (m, 2H), 6.12 (s, 2H), 3.37 (q, 8H), 3.32 (m, 2H) 2.91 (m, 1H), 2.51 (dd, 2H), 1.93 (d, 2H), 1.34 (m, 3H), 1.19 (m, 12H). ^{13}C NMR (CD$_2$Cl$_2$, 75.459 MHz): 169 (d) 158 (dd), 154, 135 (d), 111 (d), 104 (d), 100 (dd), 99, 72 (dd), 45 (t), 31, 29, 27, 25, 12.5 (q). Analyzed for C$_{28}$H$_{38}$MnN$_5$O$_2$ calculated (found): C, 63.27 (63.02); H, 7.21 (7.55); N, 13.17 (13.11).

Reaction of {[PhBP$^{iPr}_3$]Fe}$_2$(μ-N$_2$) with (salen*)Mn≡N: A solution of {[PhBP$^{iPr}_3$]Fe]}$_2$(μ-N$_2$) (15 mg, 0.014 mmol) in THF (0.8 mL) was added to solid trans-[1,2-cyclohexanediamino-N,N'-bis(4-diethylaminosalicylidene])Mn≡N (14.6 mg, 0.028 mmol). The slurry was stirred vigorously for 20 minutes and then transferred to an NMR tube equipped with a capillary tube containing O=P(OMe)$_3$ (7.3 mg, 0.052 mmol) in *d*$_8$-toluene as an internal standard. The ^{31}P {^{1}H} NMR showed a peak at 82 ppm and integration against the standard established 41% conversion to [PhBP$^{iPr}_3$]Fe≡N based upon iron. ^{1}H NMR spectra taken in THF-*d*$_8$ corroborated this result as yields of 37 ± 6% (3 experiments) were determined for [PhBP$^{iPr}_3$]Fe≡N (based upon an internal integral standard of Cp$_2$Fe). Reaction of {[PhBP$^{iPr}_3$]Fe]}$_2$(μ-N$_2$) (15 mg, 0.014 mmol) and trans-[1,2-cyclohexanediamino-N,N'-bis(4-diethylaminosalicylidene])Mn≡N (14.6 mg, 0.028 mmol) in pentane progressed much more slowly due to the low solubility of the precursors. The presence of [PhBP$^{iPr}_3$]Fe≡N was nonetheless discernable by IR spectroscopy from the signature Fe≡N vibration for [PhBP$^{iPr}_3$]Fe≡N at 1034 cm^{-1}.

---

[4] J. Du Bois, J. Hong, E. M. Carreira, M. W. Day, *J. Am. Chem. Soc*. **118**, 915 (1996).

UV-vis spectroscopy: A thawing solution of [PhBP$^{iPr}_3$]FeCl (30 mg, 0.052 mmol) in THF (5.0 mL) was added to solid Li(dbabh) (10.5 mg, 0.052 mmol) at ca. -100 ºC. The 0.01 M solution was then stirred vigorously as it was allowed to warm to room temperature for 15 minutes. From this reaction solution an aliquot of 0.4 mL was diluted to 3.0 mL (THF) in a quartz cuvette (1.3 mM) and placed in a Varian optical spectrometer for analysis. A full spectrum showing the growth of anthracene absorptions (λ = 340, 359, 378 nm) and the decay of a band (475 nm) associated with [PhBP$^{iPr}_3$]Fe(dbabh) is shown in Figure A2. The rate of decay of [PhBP$^{iPr}_3$]Fe(dbabh) was monitored by the disappearance of the band at 475 nm over a time period of 65 minutes. No discernable change in the absorption band at 475 nm was discernable after 55 minutes at which time the reaction considered complete. Plotting the $\ln(A_{initial} - A_{final})$ vs. time t (Figure 2b) established the decay of the amide to be first order with a half life of 11 minutes at 22 ºC.

Figure A2. (top panel) Optical spectrum of [PhBP$^{iPr}_3$]Fe(dbabh) (1.2 mM in THF) showing decay over time (60 min); (lower panel) ln($A_{initial} - A_{final}$) vs t indicating first order decay of [PhBP$^{iPr}_3$]Fe(dbabh).

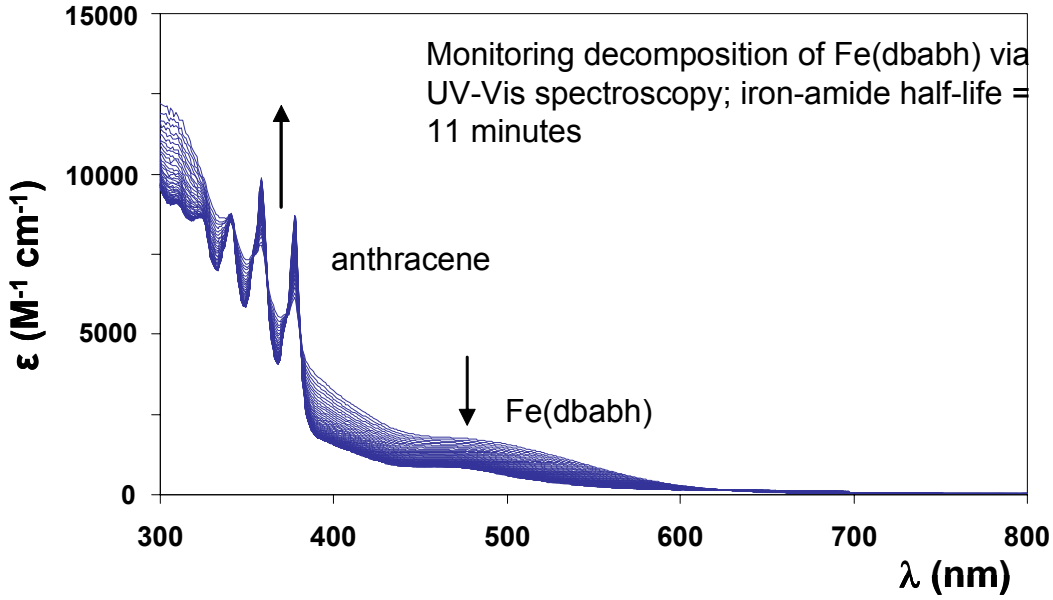

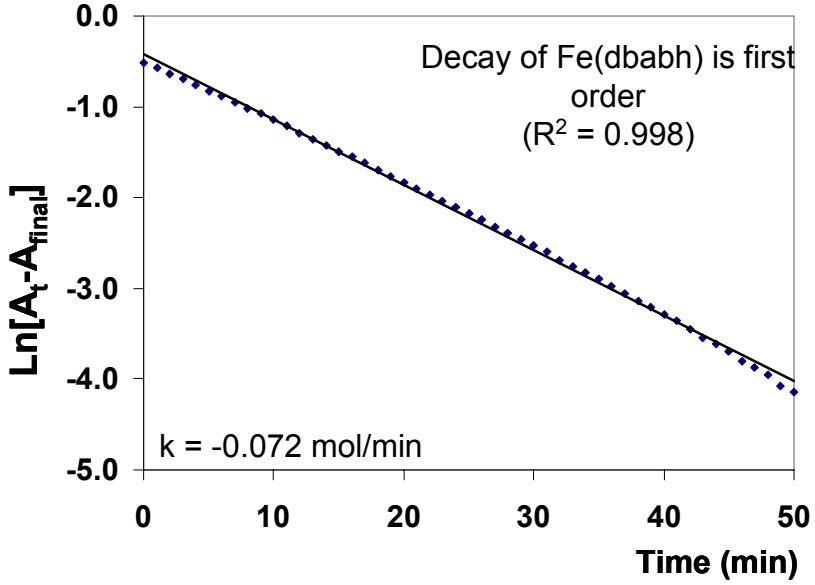

Nitride coupling under vacuum: Upon removal of volatiles under vacuum of a 0.05 M solution of $[PhBP^{iPr}_3]Fe{\equiv}N$ in C_6D_6, the nitride underwent bimolecular condensation to produce the monovalent, dinitrogen bridged complex $\{[PhBP^{iPr}_3]Fe\}_2(\mu\text{-}N_2)$ that had been previously synthesized.[5] Figure 3 (top panel) shows the ^1H NMR (C_6D_6) obtained from the nitride condensation and the lower panel displays a spectrum (^1H NMR (C_6D_6)) of the independently synthesized complex $\{[PhBP^{iPr}_3]Fe\}_2(\mu\text{-}N_2)$. Anthracene is also present in the top panel, resulting from the original $[PhBP^{iPr}_3]Fe$(dbabh) decomposition to $[PhBP^{iPr}_3]Fe{\equiv}N$.

Nitride coupling under argon: Volatiles were removed under vacuum at -35 ºC of a red solution of $[PhBP^{iPr}_3]Fe$(dbabh) that had prepared in THF as described above. The residue was trituration with pentane at -35 ºC, and the resulting solids were quickly transported to an argon-filled glove-box and reconstituted in C_6D_6 at 22 ºC to provide an ca. 0.05 M solution of $[PhBP^{iPr}_3]Fe{\equiv}N$ after 30 min. The concentration of $[PhBP^{iPr}_3]Fe{\equiv}N$ was monitored by ^1H NMR spectroscopy over a period of 8 h. As in the case of the bimolecular condensation of $[PhBP^{iPr}_3]Fe{\equiv}N$ to produce the dinitrogen bridged species $\{[PhBP^{iPr}_3]Fe\}_2(\mu\text{-}N_2)$ under vacuum, most of the $[PhBP^{iPr}_3]Fe{\equiv}N$ had decayed to $\{[PhBP^{iPr}_3]Fe\}_2(\mu\text{-}N_2)$ after this time (see Figure A4). Figure A4 shows the aryl region of the $[PhBP^{iPr}_3]Fe{\equiv}N$ ^1H NMR spectrum at t = 0 and t = 80 min, and shows the full spectrum at t = 80 min showing the presence of a small amount of $[PhBP^{iPr}_3]Fe{\equiv}N$ and a large amount of $\{[PhBP^{iPr}_3]Fe\}_2(\mu\text{-}N_2)$.

$[PhBP^{iPr}_3]Fe\text{-}N{=}PR_3$: A thawing solution of $[PhBP^{iPr}_3]FeCl$ (60 mg, 0.105 mmol) in THF (0.2 mL) was added to solid Li(dbabh) (20.9 mg, 0.105 mmol) at ca. -100 ºC. The solution was stirred vigorously and allowed to warm to room temperature, stirring for a total of 25 minutes. Solid triphenylphosphine (27.5 mg, 0.105 mmol) was added to the solution and stirred for an additional 3 hours, at which time the volatiles were removed in vacuo. The resulting orange solids were dissolved in benzene and filtered through a glass-fiber filter to remove insoluble material (LiCl). Removal of benzene in vacuo followed by storage in cold pentane (-33 ºC) for 36 h precipitated the product $[PhBP^{iPr}_3]Fe\text{-}N{=}PPh_3$, which contained a ca. 10% anthracene by ^1H NMR. The product was analyzed spectroscopically: ^1H NMR (C_6D_6, 300 MHz): δ 51.8, 48.4 23.4, 22.8, 20.7, 8.29, 7.37, 7.08, -5.4, -25.5, -47.6. Evans method (C_6D_6): 4.99 μ_B. IR (C_6H_6/KBr): $\upsilon_{P=N}$ 1223 cm^{-1}. ES-MS (Electrospray): (Ph_3PNH) m/z 277, found $(C_6H_5)_3PNH{+}H)^+$ m/z 278. $[PhBP^{iPr}_3]Fe(N{=}PEt_3)$: Using an analogous method as described above, liquid triethylphosphine (12.5 mg, 0.105 mmol) was added to a solution of in situ generated $[PhBP^{iPr}_3]Fe{\equiv}N$ (0.105 mmol). ^1H NMR (C_6D_6, 300 MHz): δ 84.3, 48.1, 47.2, 22.7, 20.7, 3.56, -6.6, -23.6, -29.2, -47.5. IR (C_6H_6/KBr): $\upsilon_{P=N}$ 1214 cm^{-1}. ES-MS (Electrospray): (Et_3PNH) m/z 119, found $(C_2H_5)_3PNH{+}H)^+$ m/z 120.

Reaction of $[PhBP^{iPr}_3]Fe{\equiv}N$ with Cp_2Co and $[LutH][BPh_4]$. A thawing solution of $[PhBP^{iPr}_3]FeCl$ (20 mg, 0.035 mmol) in THF (0.3 mL) was added to solid Li(dbabh) (7.0 mg, 0.035 mmol) at ca. -100 ºC. The solution was stirred vigorously and allowed to warm to -35 ºC. The volatiles were removed in vacuo while maintaining the reaction vessel at -35 ºC. The solids were washed with cold pentane and dried under vacuum at -35 ºC to afford $[PhBP^{iPr}_3]Fe$(dbabh) as a red solid, which was then dissolved in 0.8 mL of C_6D_6 and filtered through a glass-fiber filter to remove insoluble material. The filtrate was allowed to stand for 25 minutes at room

[5] T. A. Betley, J. C. Peters, *J. Am. Chem. Soc.* **125**, 10782 (2003).

temperature and the presence of cleanly generated [$PhBP^{iPr}_3$]Fe≡N was verified by ^{31}P and ^{1}H NMR analysis. The solution was added to a round-bottomed flask fitted with a Teflon valve containing solid Cp_2Co (23.2 mg, 0.12 mmol; 3.5 eq.) and solid lutidinium tetraphenylborate [LutH][BPh_4] (52.2 mg, 0.12 mmol; 3.5 eq.). Yellow precipitate was evident within minutes after the addition of the nitride solution to the solid $CoCp_2$ and [LutH][BPh_4]. After stirring for two hours, the reaction volatiles were vacuum-transferred onto a frozen ethereal solution containing 10 equivalents of HCl (1.0 M, Et_2O) in a 25 mL flask fitted with a Teflon valve. NaO^tBu (10 mg, 0.11 mmol) in THF (0.2 mL) was added to the original reaction flask and the residue was stirred for an additional 20 minutes. The volatiles were then again transferred into the flask containing the HCl solution. The vac-transferred products were stirred for 20 minutes and then the volatile components were removed. ^{1}H NMR analysis (d_6-DMSO) of the resulting solids that remained showed the presence of LutHCl and NH_4Cl as the principal components. Integration against an integral standard of mesitylene (4.2 mg, 0.035 mmol) revealed yields of 41% and 45% NH_4Cl in two independent experimental runs.

Figure A3. ^{1}H NMR spectrum indicating $[PhBP^{iPr}_{3}]Fe{\equiv}N$ coupling to generate $\{[PhBP^{iPr}_{3}]Fe\}_{2}(\mu\text{-}N_{2})$ upon concentration under vacuum (axis units in ppm).

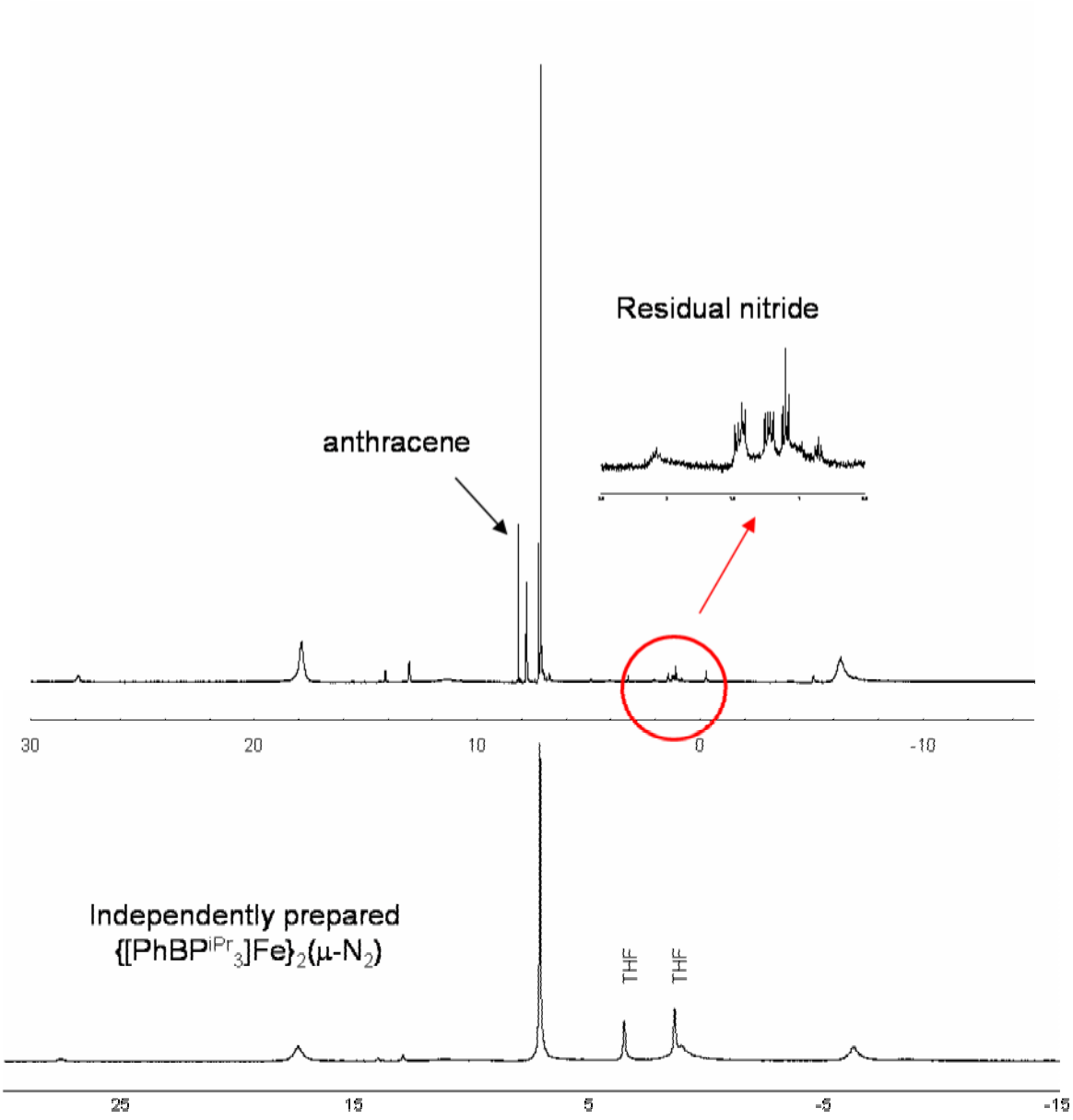

Figure A4. ^{1}H NMR spectra illustrating nitride coupling reaction under argon.

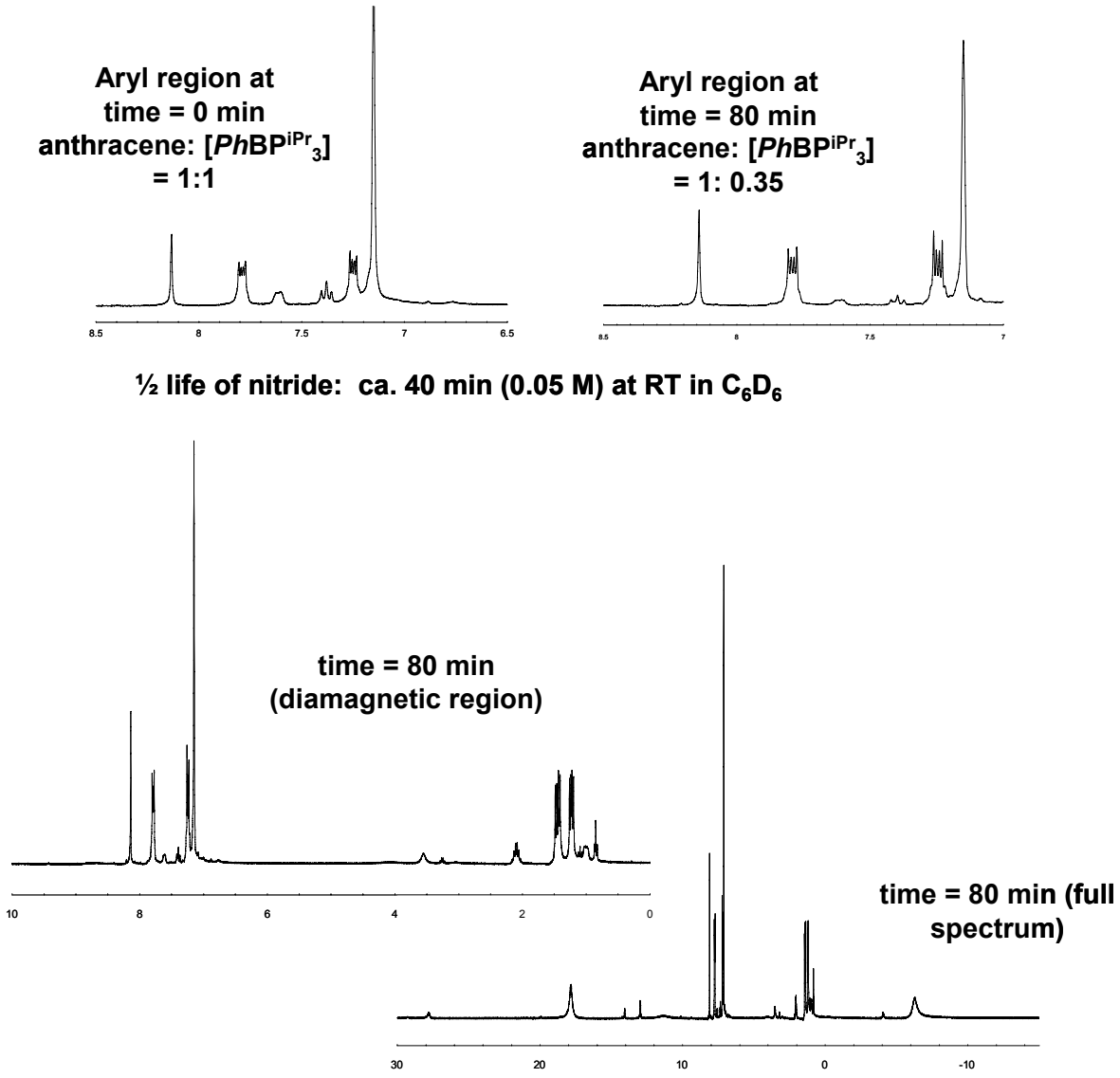

Electronic Structure Calculations. A hybrid density functional calculation was performed for [PhBP$^{iPr}_3$]Fe≡N using the Jaguar package (version 5.0, release 20). The calculation employed B3LYP with LACVP** as the basis set. A geometry optimization was carried out starting from coordinates based on the solid-state structure of [PhBP$^{iPr}_3$]Fe≡NAd (with the adamantly substituent removed) as the initial HF guess.[5] No symmetry constraints were imposed and the calculation was performed assuming a singlet ground electronic state. Figure A5 shows the geometry optimized structure predicted from the calculation.

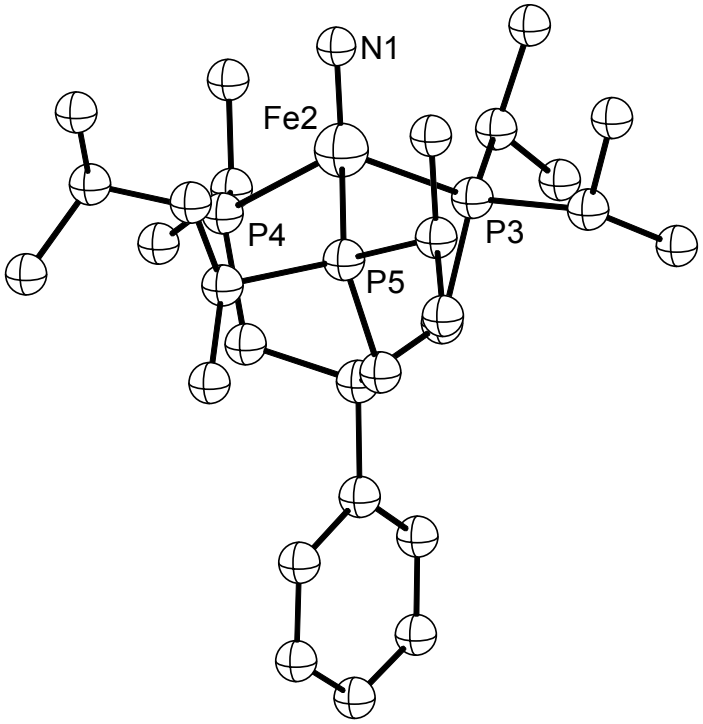

Bond lengths (Å)
Fe2-N1: 1.490
Fe2-P3: 2.275
Fe2-P4: 2.286
Fe2-P5: 2.275

Bond Angles (º):
N1-Fe2-P3: 116.84
N1-Fe2-P4: 118.58
N1-Fe2-P5: 117.38
P3-Fe2-P4: 99.23
P3-Fe2-P5: 100.85
P4-Fe2-P5: 100.67

Figure A5. DFT predicted structure for [PhBP$^{iPr}_3$]Fe≡N.

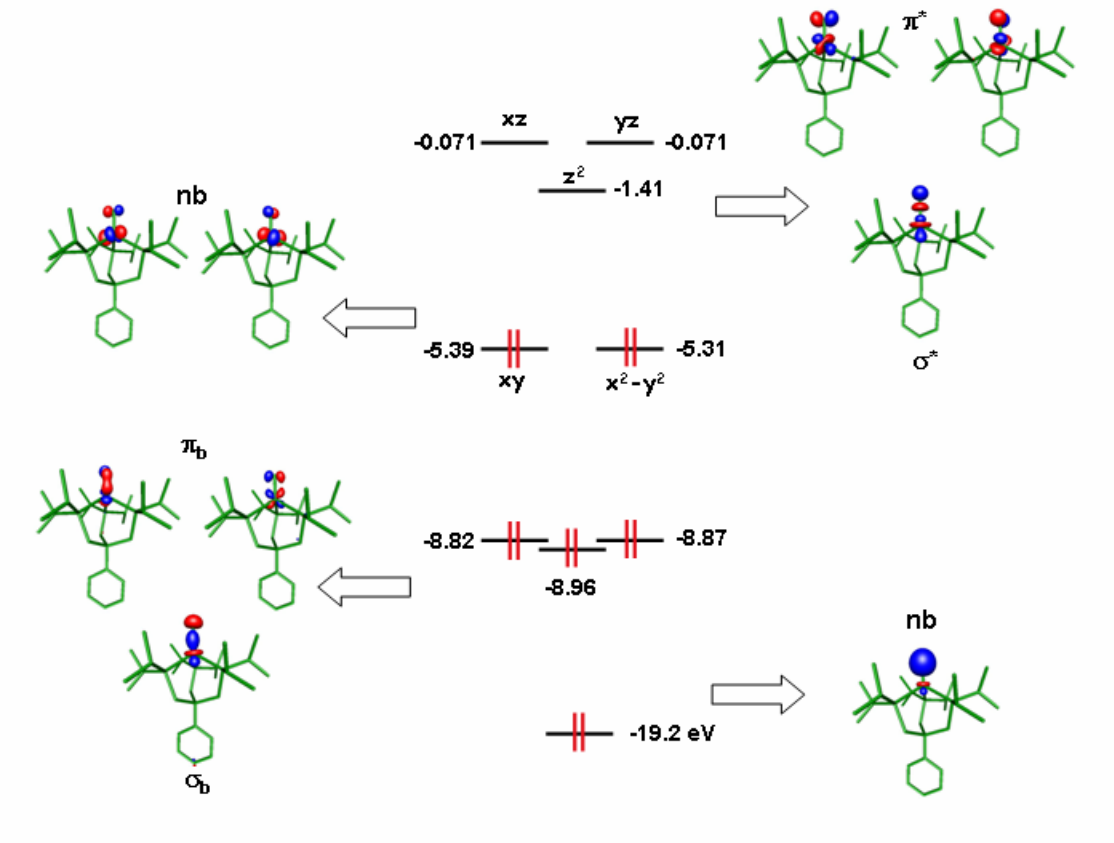

Figure A6. Theoretically predicted geometry and electronic structure (DFT, JAGUAR 5.0, B3LYP/LACVP**) for the complex [PhBP$^{iPr}_3$]Fe≡N. A singlet ground state was applied as the only constraint. Lobal representations correspond to the orbitals indicated by the directional arrows. Noteworthy structural parameters: Fe-P = 2.28, 2.28, 2.29 Å; N-P-Fe = 117, 117, 119º; P-Fe-P = 99, 101, 101º; Fe-N = 1.490 Å. See Supporting Information for further details.

Figure A7. Displacement ellipsoid (50%) representation of $\{[PhBP^{iPr}_3]Fe\}_2(\mu\text{-}N_2)$.

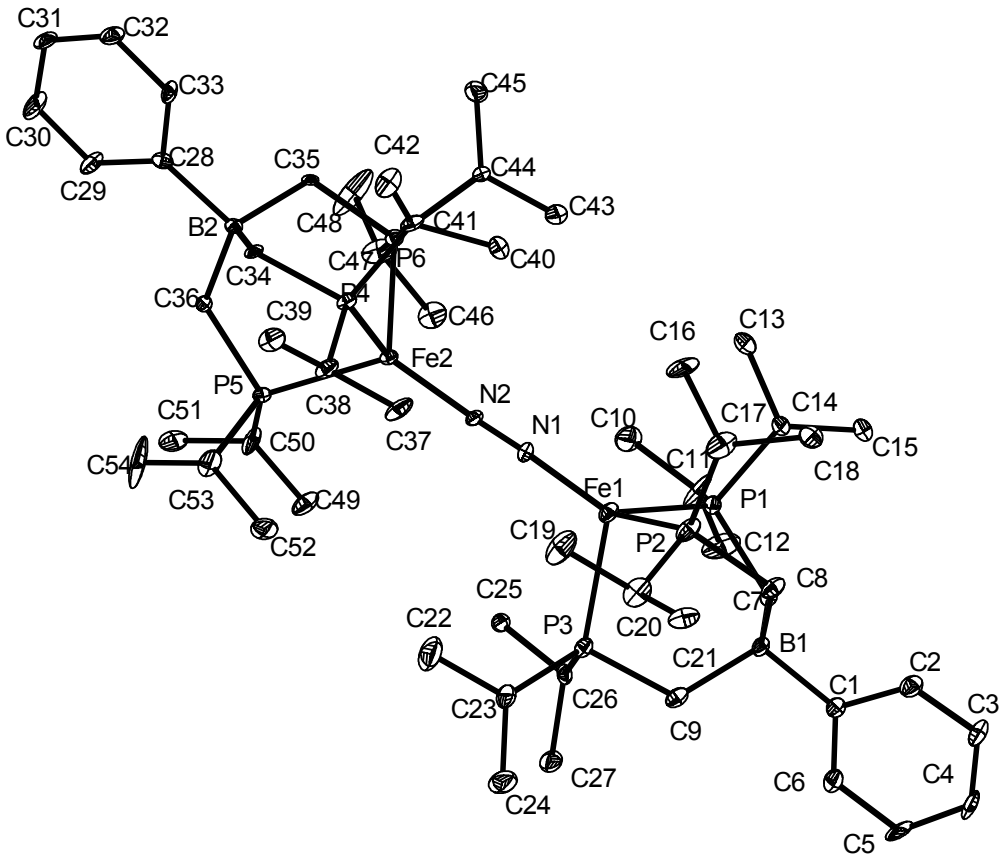

Table A1. Crystal data and structure refinement for $\{[PhBP^{iPr}_3]Fe\}_2(\mu\text{-}N_2)$.

Identification code	tab43	
Empirical formula	$C_{54}H_{97}B_2Fe_2N_2P_6$	
Formula weight	1093.48	
Temperature	100(2) K	
Wavelength	Orthorhombic	
Space group	Pca2(1)	
Unit cell dimensions	a = 26.3682(17) Å	α= 90°.
	b = 14.3569(9) Å	β= 90°.
	c = 32.485(2) Å	γ = 90°.
Volume	12297.9(13) Å^3	
Z	8	
Density (calculated)	1.181 Mg/m^3	
Absorption coefficient	0.662 mm^{-1}	
F(000)	4696	
Crystal size	0.185 x 0.185 x 0.315 mm^3	
Theta range for data collection	1.25 to 24.84°	
Index ranges	-31<=h<=30, -16<=k<=16, -37<=l<=38	
Reflections collected	96135	
Independent reflections	19520 [R(int) = 0.0622]	
Completeness to theta = 24.84°	95.0 %	
Absorption correction	None	
Refinement method	Full-matrix least-squares on F^2	
Data / restraints / parameters	19520 / 1 / 1232	
Goodness-of-fit on F^2	1.645	
Final R indices [I>2σ (I)]	R1 = 0.0504, wR2 = 0.0973	
R indices (all data)	R1 = 0.0758, wR2 = 0.1019	
Absolute structure parameter	0.603(16)	
Largest diff. peak and hole	0.890 and -0.459 e.Å^{-3}	

Special Refinement Details

Refinement of F^2 against ALL reflections. The weighted R-factor (*w*R) and goodness of fit (S) are based on F^2, conventional R-factors (R) are based on F, with F set to zero for negative F^2. The threshold expression of $F^2 > 2\sigma(F^2)$ is used only for calculating R-factors(gt) etc. and is not relevant to the choice of reflections for refinement. R-factors based on F^2 are statistically about twice as large as those based on F, and R-factors based on ALL data will be even larger.

All esds (except the esd in the dihedral angle between two l.s. planes) are estimated using the full covariance matrix. The cell esds are taken into account individually in the estimation of esds in distances, angles and torsion angles; correlations between esds in cell parameters are only used when they are defined by crystal symmetry. An approximate (isotropic) treatment of cell esds is used for estimating esds involving l.s. planes.

The crystal was twinned and refined as such (BASF = 0.64).

Table A2. Pertinent bond lengths [Å] and angles [°] for $\{[PhBP^{iPr}_3]Fe\}_2(\mu\text{-}N_2)$.

N(1)-N(2)	1.138(6)
N(1)-Fe(1)	1.811(5)
N(2)-Fe(2)	1.818(5)
Fe(1)-P(3)	2.3395(18)
Fe(1)-P(1)	2.3497(17)
Fe(1)-P(2)	2.3944(18)
P(1)-C(11)	1.826(6)
P(1)-C(7)	1.834(6)
P(1)-C(14)	1.866(6)
P(2)-C(8)	1.815(6)
P(2)-C(17)	1.853(7)
P(2)-C(20)	1.853(7)
P(3)-C(9)	1.844(6)
P(3)-C(23)	1.849(6)
P(3)-C(26)	1.860(6)
B(1)-C(1)	1.628(10)
B(1)-C(9)	1.658(8)
B(1)-C(8)	1.668(9)
B(1)-C(7)	1.683(8)
C(1)-C(6)	1.386(9)
C(1)-C(2)	1.396(9)
C(2)-C(3)	1.415(9)
C(2)-H(2)	0.9500
C(3)-C(4)	1.346(10)
C(3)-H(3)	0.9500
C(4)-C(5)	1.391(11)
C(4)-H(4)	0.9500
C(5)-C(6)	1.405(9)
C(5)-H(5)	0.9500
C(6)-H(6)	0.9500
C(7)-H(7A)	0.9900
C(7)-H(7B)	0.9900
C(8)-H(8A)	0.9900
C(8)-H(8B)	0.9900
C(9)-H(9A)	0.9900
C(9)-H(9B)	0.9900
C(10)-C(11)	1.514(8)
C(10)-H(10A)	0.9800
C(10)-H(10B)	0.9800
C(10)-H(10C)	0.9800
C(11)-C(12)	1.456(9)
C(11)-H(11)	1.0000
C(12)-H(12A)	0.9800
C(12)-H(12B)	0.9800
C(12)-H(12C)	0.9800
C(13)-C(14)	1.526(9)
C(13)-H(13A)	0.9800
C(13)-H(13B)	0.9800
C(13)-H(13C)	0.9800
C(14)-C(15)	1.486(8)
C(14)-H(14)	1.0000
C(15)-H(15A)	0.9800

Figure A8. Displacement ellipsoid (50%) representation of $[PhBP^{iPr}_3]FeNPh_2$.

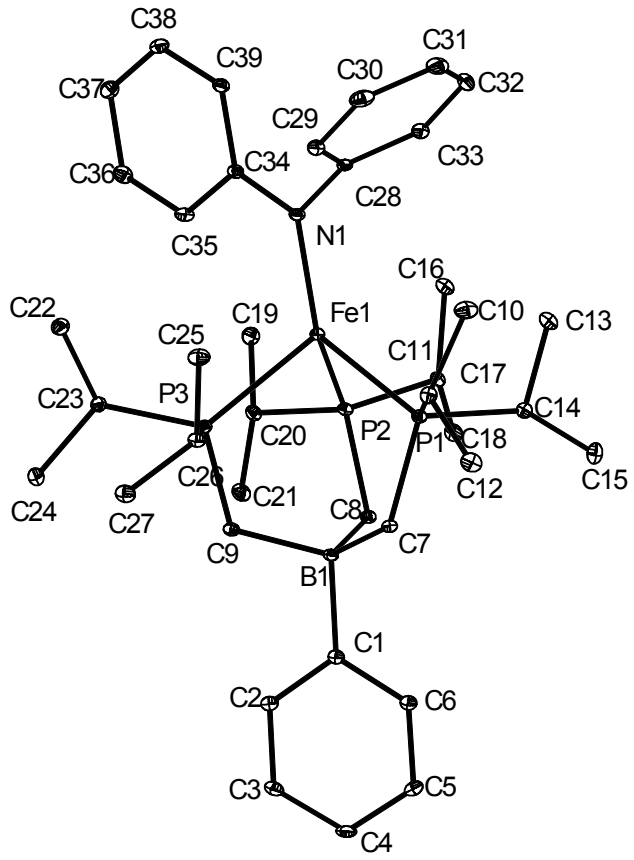

Table A3. Crystal data and structure refinement for $[PhBP^{iPr}_3]FeNPh_2$.

Identification code	tab47
Empirical formula	$C_{39}H_{63}BFeNP_3$
Formula weight	705.47
Temperature	100(2) K
Wavelength	0.71073 Å
Crystal system	Triclinic
Space group	P-1
Unit cell dimensions	a = 11.0240(9) Å α= 87.377(2)°
	b = 13.4574(11) Å β= 75.6030(10)°
	c = 13.7499(11) Å γ = 83.956(2)°
Volume	1964.4(3) $Å^3$
Z	2
Density (calculated)	1.193 Mg/m^3
Absorption coefficient	0.533 mm^{-1}
F(000)	760
Crystal size	0.10 x 0.15 x 0.41 mm^3
Theta range for data collection	1.52 to 30.76°
Index ranges	-15<=h<=15, -18<=k<=19, -19<=l<=19
Reflections collected	44708
Independent reflections	11014 [R(int) = 0.0855]
Completeness to theta = 30.76°	89.9 %
Absorption correction	None
Refinement method	Full-matrix least-squares on F^2
Data / restraints / parameters	11014 / 0 / 418
Goodness-of-fit on F^2	1.273
Final R indices [I>2σ (I)]	R1 = 0.0448, wR2 = 0.0797
R indices (all data)	R1 = 0.0841, wR2 = 0.0906
Largest diff. peak and hole	0.658 and -0.432 $e.Å^{-3}$

Special Refinement Details

Refinement of F^2 against ALL reflections. The weighted R-factor (*w*R) and goodness of fit (S) are based on F^2, conventional R-factors (R) are based on F, with F set to zero for negative F^2. The threshold expression of $F^2 > 2\sigma(F^2)$ is used only for calculating R-factors(gt) etc. and is not relevant to the choice of reflections for refinement. R-factors based on F^2 are statistically about twice as large as those based on F, and R-factors based on ALL data will be even larger.

All esds (except the esd in the dihedral angle between two l.s. planes) are estimated using the full covariance matrix. The cell esds are taken into account individually in the estimation of esds in distances, angles and torsion angles; correlations between esds in cell parameters are only used when they are defined by crystal symmetry. An approximate (isotropic) treatment of cell esds is used for estimating esds involving l.s. planes.

Table A4. Pertinent bond lengths [Å] and angles [°] for $[PhBP^{iPr}_3]FeNPh_2$.

Fe(1)-N(1)	1.9527(15)	C(4)-H(4)	0.9500
Fe(1)-P(3)	2.4432(6)	C(5)-C(6)	1.397(3)
Fe(1)-P(1)	2.4623(6)	C(5)-H(5)	0.9500
Fe(1)-P(2)	2.4669(6)	C(6)-H(6)	0.9500
N(1)-C(34)	1.394(2)	C(7)-H(7A)	0.9900
N(1)-C(28)	1.429(2)	C(7)-H(7B)	0.9900
P(1)-C(7)	1.8343(18)	C(8)-H(8A)	0.9900
P(1)-C(14)	1.859(2)	C(8)-H(8B)	0.9900
P(1)-C(11)	1.8581(19)	C(9)-H(9A)	0.9900
P(2)-C(8)	1.8291(18)	C(9)-H(9B)	0.9900
P(2)-C(17)	1.860(2)	C(10)-C(11)	1.532(3)
P(2)-C(20)	1.8701(19)	C(10)-H(10A)	0.9800
P(3)-C(9)	1.8217(19)	C(10)-H(10B)	0.9800
P(3)-C(26)	1.861(2)	C(10)-H(10C)	0.9800
P(3)-C(23)	1.864(2)	C(11)-C(12)	1.533(3)
B(1)-C(1)	1.649(3)	C(11)-H(11)	1.0000
B(1)-C(9)	1.670(3)	C(12)-H(12A)	0.9800
B(1)-C(8)	1.673(3)	C(12)-H(12B)	0.9800
B(1)-C(7)	1.673(3)	C(12)-H(12C)	0.9800
C(1)-C(6)	1.395(3)	C(13)-C(14)	1.536(3)
C(1)-C(2)	1.406(3)	C(13)-H(13A)	0.9800
C(2)-C(3)	1.387(3)	C(13)-H(13B)	0.9800
C(2)-H(2)	0.9500	C(13)-H(13C)	0.9800
C(3)-C(4)	1.379(3)	C(14)-C(15)	1.530(3)
C(3)-H(3)	0.9500	C(14)-H(14)	1.0000
C(4)-C(5)	1.374(3)	C(15)-H(15A)	0.9800